The Charge and Spin Thermoelectric Properties across Double Quantum Dots Serially Coupled to Ferromagnetic Leads: The Case of Parallel Magnetic Configuration

M. A. Najdi[1,*], J. M. AL-Mukh[2], H. A. Jassem[1]

1. Department of Physics, Collage of Science, University of Basrah, Basra, Iraq
2. Department of Physics,, Collage of Education for Pure Science, University of Basrah, Basra, Iraq

*Corresponding author E-mail: **mohammed_a_najdi@yahoo.com**

Doi:10.29072/basjs.20220106

ARTICLE INFO

Keywords

Double quantum dots,

Ferromagnetic leads,

Figure of merit, Parallel magnetic configuration, Thermoelectric materials.

ABSTRACT

In present work, the charge and spin thermoelectric properties of double quantum dots system connected to ferromagnetic leads with collinear magnetic configurations will be studied in the linear response regime. Our results are calculated in a strong interdot coupling regime by taking into consideration all parameters affecting the system such as interaction between dots and their coupling to the leads, intradot Coulomb correlation energy and spin-polarization on the leads. It is found that in the parallel magnetic configuration, the thermoelectric efficiency can reach a large value around the spin-down resonance levels when the tunneling coupling between the quantum dots and the leads for the spin-down electrons are small, which leads to the pure spin Seebeck contribution. As a result, this system can generate a spin-polarized current. The value of the spin figure of merit is enhanced by increasing the spin-polarization and decreasing the correlation energy.

Received 10 Des 2022; Received in revised form 3 Feb 2022; Accepted 25 Feb 2022, Published 30 Apr 2022

1. Introduction

In the last few years, the reconnaissance of high performance thermoelectric materials has attracted a lot of academic and applied attention. The challenge for the development of these materials is to design the close relationship of thermoelectric physical processes to electrical conductivity (G), Seebeck coefficient (S) and thermal conductivity (κ) of crystalline systems. The efficiency of thermoelectric devices is strongly correlated with the figure of merit (ZT) of thermoelectric materials. High electrical conductivity, large Seebeck coefficient and low thermal conductivity are all necessary for access to high performance thermoelectric materials. Developments in thermoelectric efficiency have shown that it can be controlled by suppressing thermal conductivity during nanostructure design. The coefficients like S, G, κ and absolute temperature (T) are strongly related to one another the value of ZT for bulk materials has been found to be limited to 1, due to the increase in G and κ. The value of ZT greater than 1 is required for energy applications, where this value is accessible through nanotechnology, due to the high mean free path of the phonon as compared to the electron. That the transport of phonons and electrons can be easily controlled in nanostructures as compared to bulk materials [1]. The use of nanostructures breaks the link between thermal and electrical properties through the mechanics of scattering and thus enhances the value of ZT, S and G. κ can be suppressed by phonons in nanostructures in order to obtain high G and then better ZT. However, ZT increases with the density of states, the decrease in material dimensions (such that, 2D quantum wells, 1D quantum wire and 0D quantum dots) causes dramatic differences in the electronic density of states that provide opportunities to independently control physical parameters. Thereby, increasing ZT beyond 1 is a challenging task.

In electronics that depends on the electron spin (i.e. Spintronics), which refers to the science and technology of controlling the electron's charge and intrinsic angular momentum (the electron spin), thermoelectric technology has received wide attention in many fields, for example: solar heat utilization, waste heat recovery and thermal management in processors [2-4]. The low-dimensional thermoelectric system was developed with the help of these two concepts, so ZT can be increased either by reducing κ or by increasing the energy barriers. In the absence of phonon conductance, a single quantum dot (QD) junction system can have a very impressive ZT, according to some theoretical works [5-7]. It is critical to consider connected double quantum dots (DQDs) in order to reduce the temperature gradient across the QD junction [8,9]. The DQDs

junction system's thermal resistance can be higher than that of a single QD system. The DQDs system can sustain a considerable temperature difference across the junction because of this property. Among all the candidates for low-dimensional thermoelectric materials, DQDs systems are recommended for their interesting thermoelectric properties due to their scalability and high degree of tunability [10-12]. Thus, DQDs have already paved their way to become underlying devices of spintronics not only because of beautiful physics emerging in those systems, but, more importantly, due to possible future applications and due to the possibility of manipulation of a single spin [13-15]. DQDs systems may display some new thermoelectric phenomena as they reveal a variety of different interference effects, including Fano resonances. The Fano effect occurs in DQDs due to quantum interference of waves resonantly transmitted through a discrete level and those transmitted non-resonantly through continuum of states. The discovery of the spin Seebeck effect stimulated experimental and theoretical interest in the so called "spin caloritronics" [16-18]. Spin caloritronics, the combination of thermoelectrics with spintronics, exploiting both the intrinsic spin of electron and its associated magnetic moment in addition to its fundamental electronic charge and heat, is an emerging technology mainly in the development of low power consumption technology. Although spin caloritronics are as old as spin electronics, they have been poorly investigated and have been dormant for many years except for some experimental work on the thermoelectric properties of multi magnetic layers in current in-plane geometry [19,20]. In this work, we investigated the charge and spin thermoelectric properties across DQDs serially coupled to ferromagnetic leads in the case of parallel magnetic configuration. This is achieved by employing an approach that incorporates a uniform treatment of electron dynamics in the system under investigation; the nonequilibrium Green's function formalism is employed for this purpose [21].

2. Model and Formalism

The system under study can be described by using Anderson Hamiltonian, which takes into consideration exchange interactions and all couplings as follows [22];

$$H = H_{DQDs} + H_{leads} + H_{QD-QD} + H_{DQDs-Leads} \quad (1)$$

DQDs Hamiltonian with electronic level E_{di}^{σ} $(i = 1,2)$ and spin σ $(\uparrow,\downarrow)$, is denoted by the first term in equation 1, (first two terms in equation 2),

$$H = \sum_{\sigma}\sum_{i=1}^{2} E_{di}^{\sigma} n_{di}^{\sigma} + \sum_{i=1}^{2} U_i n_{di}^{\sigma} n_{di}^{-\sigma} + \sum_{\sigma}\sum_{\alpha}\sum_{k_\alpha} E_{k_\alpha}^{\sigma} n_{k_\alpha}^{\sigma} + \sum_{\sigma}\{(V_{12}\, C_{d1}^{\sigma\dagger} C_{d2}^{\sigma} + H.c.) + \frac{1}{2} J_{\circ}\, (C_{d1}^{\sigma\dagger} C_{d2}^{\sigma\dagger} C_{d1}^{\sigma} C_{d2}^{\sigma} + H.c.)\} + \sum_{\sigma}\sum_{\alpha}\sum_{i=1}^{2}\sum_{k_\alpha} (V_{ik_\alpha}^{\sigma} C_i^{\sigma\dagger} C_{k_\alpha}^{\sigma} + H.c.) \quad 2$$

n_{di}^{σ} are the corresponding occupation numbers, since $n_{di}^{\sigma} = C_{di}^{\sigma\dagger} C_{di}^{\sigma}$, C_{di}^{σ} $(C_{di}^{\sigma\dagger})$ being the annihilation (creation) operator of QD electronic state i with spin σ. The energies of the dots levels are defined in the following equations;

$$E_{d1}^{\sigma} = E_1 + U_1 n_{d1}^{-\sigma} - J n_{d2}^{\sigma}$$
$$E_{d2}^{\sigma} = E_2 + U_2 n_{d2}^{-\sigma} - J n_{d1}^{\sigma} \quad 3$$

U_i represents the intradot Coulomb correlation on ith QD sites. E_i is the effective energy level of dot i, while J represents the spin-spin exchange interaction. The electrons of the leads are described by the second term in equation 1, (third term in equation 2). $E_{k_\alpha}^{\sigma}$ denotes the single electron energy levels in the leads $(\alpha \equiv L, R)$ with momentum k_α and spin σ, $n_{k_\alpha}^{\sigma}$ are the corresponding occupation numbers. The Hamiltonian due to interaction between the terms for two dots is described by the third term in equation 1, (fourth and five terms in equation 2), where the hopping energy between the dots is V_{12} and the noneffective spin exchange interaction is $J_{\circ}$. Finally, the tunneling energy between each dot and leads is given by the last term in equation 1, (sixth term in equation 2), $C_{k_\alpha}^{\sigma}$ $(C_{k_\alpha}^{\sigma\dagger})$ being the annihilation (creation) operator of an electron with momentum k_α, where the tunneling spin-dependent amplitude between each ferromagnetic lead and the nearest dot is given by $V_{ik_\alpha}^{\sigma}$. Fig. (1) shows schematic energy diagram for the system of a DQDs in series configuration.

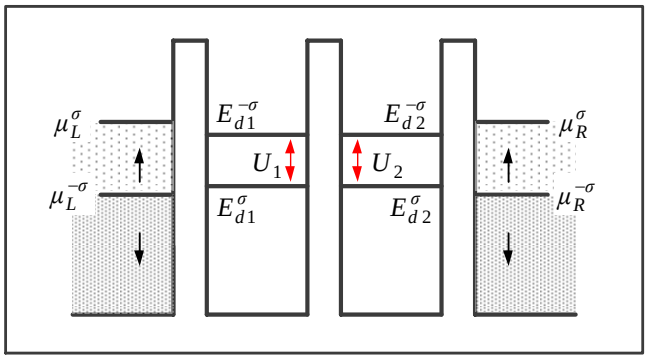

Figure1: Schematic energy diagram for the system of serially DQDs: the case of parallel magnetic configuration.

Using the following relations, the spin-dependent formula for the occupation numbers of the DQDs energy levels has already been determined [23];

$$n_{di}^{\sigma} = \int_{-\infty}^{\mu_{\alpha}^{\sigma}} \rho_{i\alpha}^{\sigma}(E)\, f_{\alpha}^{\sigma}(E,T_{\alpha})dE \quad ; \quad f_{\alpha}^{\sigma}(E,T_{\alpha}) = \frac{1}{e^{(E-\mu_{\alpha}^{\sigma})/k_B T_{\alpha}}+1} \qquad 4$$

$f_{\alpha}^{\sigma}(E,T_{\alpha})$ is the Fermi distribution function in the lead α and μ_{α}^{σ} is the chemical potential of the lead α. The localized density of states on the ith QD with spin σ that connected to the lead α can be defined in term of Green's functions [24];

$$\rho_{i\alpha}^{\sigma}(E) = -\frac{1}{\pi}\,\mathrm{Im}\, G_{i\alpha}^{\sigma}(E) \qquad 5$$

$\mathrm{Im}\, G_{i\alpha}^{\sigma}(E)$ are the imaginary components of Green's functions, which are given by [25];

$$G_{1L}^{\sigma}(E) = \frac{1}{2}\left\{\frac{(1+W_1^{\sigma}/V_1^{\sigma})}{(E-E_{1+}^{\sigma})+\mathrm{i}\Gamma_{1L}^{\sigma}} + \frac{(1-W_1^{\sigma}/V_1^{\sigma})}{(E-E_{1-}^{\sigma})+\mathrm{i}\Gamma_{1L}^{\sigma}}\right\} \qquad 6a$$

$$G_{2R}^{\sigma}(E) = \frac{1}{2}\left\{\frac{(1-W_2^{\sigma}/V_2^{\sigma})}{(E-E_{2+}^{\sigma})+\mathrm{i}\Gamma_{2R}^{\sigma}} + \frac{(1+W_2^{\sigma}/V_2^{\sigma})}{(E-E_{2-}^{\sigma})+\mathrm{i}\Gamma_{2R}^{\sigma}}\right\} \qquad 6b$$

$\Gamma_{i\alpha}^{\sigma}$ is level broadening due to coupling interaction between the ith QD energy levels and the lead continuum energy levels. In the wide band limit, the level broadening becomes energy independent [26]. The "molecular" energy levels $E_{i\pm}^{\sigma}$ are defined as,

$$E_{i\pm}^{\sigma} = E_i + U_i n^{-\sigma} - J n^{\sigma} \pm V_i^{\sigma} \qquad 7$$

Where,

$$n^{\sigma} = \frac{n_{d1}^{\sigma} + n_{d2}^{\sigma}}{2} \quad ; \quad V_i^{\sigma} = \sqrt{V_{12}^2 + (W_i^{\sigma})^2} \tag{8}$$

$$W_i^{\sigma} = U_i M^{-\sigma} + J M^{\sigma} \quad ; \quad M^{\sigma} = \frac{n_{d1}^{\sigma} - n_{d2}^{\sigma}}{2} \tag{9}$$

Substituting equation 6 in equation 5, the localized density of states on the DQDs takes the following form;

$$\rho^{\sigma}(E) = \sum_{j=+,-} \sum_{i=1,2} \sum_{\alpha} K_{ij}^{\sigma} \rho_{i\alpha j}^{\sigma}(E) \tag{10}$$

With $j \equiv +, -$, if $i = 1$ then $\alpha \equiv L$ and if $i = 2$ then $\alpha \equiv R$, and;

$$\rho_{ij}^{\sigma}(E) = \frac{\Gamma_{i\alpha}^{\sigma}}{(E - E_{ij}^{\sigma})^2 + (\Gamma_{i\alpha}^{\sigma})^2} \tag{11}$$

For simplicity, in equation 10, reduced functions for K_{ij}^{σ} are used,

$$K_{1j}^{\sigma} = \frac{1}{2\pi}\left(1 + j\frac{W_1^{\sigma}}{V_1^{\sigma}}\right) \quad ; \quad K_{2j}^{\sigma} = \frac{1}{2\pi}\left(1 - j\frac{W_2^{\sigma}}{V_2^{\sigma}}\right) \tag{12}$$

The integral in equation 4 have been solved analytically using the Sommerfeld expansion [27,28]. To obtain the occupation numbers of quantum dots energy levels and the "molecular orbitals energies" of DQDs, equations 4 and 7 are solved self-consistently, for more details see Refs. [29,30]. For the purpose of access to charge and spin thermoelectric coefficients we need to find all the relevant transport integrals related to these coefficients, i.e. L_0^{σ}, L_1^{σ} and L_2^{σ}, these integrals have general definitions that are given by [31,32]:

$$L_n^{\sigma} = \frac{1}{h}\int dE \ (E - \mu)^n \left(-\frac{\partial f(E,T)}{\partial E}\right)\tau^{\sigma}(E) \tag{13}$$

$\tau^{\sigma}(E)$ denotes the energy dependent transmission function for electron with spin σ, which is given by [33],

$$\tau^{\sigma}(E) = 2\pi\Gamma^{\sigma}\,\rho^{\sigma}(E) \quad ; \quad \Gamma^{\sigma} = \frac{\Gamma_{1L}^{\sigma}\Gamma_{2R}^{\sigma}}{(\Gamma_{1L}^{\sigma} + \Gamma_{2R}^{\sigma})} \tag{14}$$

To solve all the integrals in equation 13 we also use Sommerfeld expansion with $n = 0,1,2$, then:

$$L_n^\sigma \cong N^\sigma(E) + \frac{\pi^2}{6}\ (k_B T)^2 \frac{d^2 N^\sigma(E)}{dE^2}\bigg|_\mu \qquad 15$$

With $N^\sigma(E) = (E-\mu)^n\ \tau^\sigma(E)$. Finally, equation 15 are solved analytically to get L_n^σ;

$$L_0^\sigma \cong \frac{1}{h}\left\{\tau^\sigma(E) + \frac{\pi^2 (k_B T)^2}{6}\frac{d^2\tau^\sigma(E)}{dE^2}\right\}\bigg|_{\mu_{eq}} \qquad 16$$

$$L_1^\sigma \cong \frac{1}{h}\left\{(E-\mu_\alpha^\sigma)\ \tau^\sigma(E) + \frac{\pi^2 (k_B T)^2}{6}\left[(E-\mu_\alpha^\sigma)\frac{d^2\tau^\sigma(E)}{dE^2} + 2\frac{d\tau^\sigma(E)}{dE}\right]\right\}\bigg|_{\mu_{eq}} \qquad 17$$

$$L_2^\sigma \cong \frac{1}{h}\left\{(E-\mu_\alpha^\sigma)^2\ \tau^\sigma(E) + \frac{\pi^2 (k_B T)^2}{6}\left[2\ \tau^\sigma(E) + 4(E-\mu_\alpha^\sigma)\frac{d\tau^\sigma(E)}{dE} + (E-\mu_\alpha^\sigma)^2\ \frac{d^2\tau^\sigma(E)}{dE^2}\right]\right\}\bigg|_{\mu_{eq}} \qquad 18$$

μ_{eq} equals to the chemical potential of the lead α and spin σ. Then the charge Seebeck coefficient can be expressed as following [34-38];

$$S_{ch} = \frac{-1}{2eT}\sum_\sigma (L_1^\sigma / L_0^\sigma) \qquad 19$$

The thermopower (or Seebeck coefficient) is calculated at the condition ($I_{sp} = 0$, $I_{ch} = 0$), or in equivalent manner at the condition that charge current equal to zero at each spin channel, then the charge and spin-dependent thermopower are given by:

$$S_{ch} = \frac{1}{2}\sum_\sigma S^\sigma \quad ; \quad S_{sp} = \frac{1}{2}\sum_\sigma \sigma S^\sigma \qquad 20$$

Where,

$$S^{\sigma} = -\frac{1}{eT}\frac{L_1^{\sigma}}{L_0^{\sigma}} \qquad 21$$

Similarly, in the linear response regime G_{ch} and G_{sp} in terms of the transport integrals (equation 13) will be;

$$G_{ch} = e^2 \sum_{\sigma} L_0^{\sigma} \quad ; \quad G_{sp} = e^2 \sum_{\sigma} \sigma L_0^{\sigma} \qquad 22$$

On the other hand, the electronic contribution to the thermal conductance functions is given by;

$$\kappa_{el} = \sum_{\sigma} \kappa_{el}^{\sigma} \quad ; \quad \kappa_{el}^{\sigma} = \frac{1}{T}\left(L_2^{\sigma} + \frac{(L_1^{\sigma})^2}{L_0^{\sigma}}\right) \qquad 23$$

κ_{el}^{σ} is electronic contribution to the thermal conductance. In order to find charge figure of merit $Z_{ch}T$ (spin figure of merit $Z_{sp}T$), we need the thermal conductivity in addition to S_{sp} and S_{ch}. Where the dimensionless ZT depend on charge and spin are given in the following formulas:

$$Z_{ch}T = \frac{G_{ch}S_{ch}^2 T}{\kappa_{el}} \quad ; \quad Z_{sp}T = \frac{G_{sp}S_{sp}^2 T}{\kappa_{el}} \qquad 24$$

All our numerical calculations are carried out using Fortran 90 language.

3. Results and Discussion

The charge and spin thermoelectric properties are studied and investigated for the system under consideration. The corresponding charge and spin figures of merit are calculated using equations 24, which describe the heat-to-charge-voltage and the heat-to-spin-voltage conversion efficiencies of the present system when the spin accumulation on the leads is considered. This may occur when the spin-relaxation period in the leads is sufficiently long, assuming that the spin accumulation in the external leads is sufficiently long. In such a case, we have to take into account the spin splitting of the chemical potential level in both leads. As the spin accumulation on the lead is considered, the chemical potentials of the ferromagnetic leads are chosen to be $\mu_{\alpha}^{\sigma} = 0.05$ eV and $\mu_{\alpha}^{-\sigma} = -0.05$ eV for the parallel magnetic configuration. Where, μ_{eq} in equations 16, 17 and 18 are equals μ_{α}^{σ} for spin-up electrons and $\mu_{\alpha}^{-\sigma}$ for spin-down electrons of

the lead α. The calculations are accomplished in the strong interdot coupling regime, $V_{12} > \Gamma_{i\alpha}^{\pm\sigma}$ as well as $\Gamma_{i\alpha}^{\pm\sigma} > k_B T$, where $T = 20$ K with the leads spin-polarization $P = 0.3$ and 0.7 and the tunneling coupling with the leads assumed to be in the form $\Gamma_{i\alpha}^{\pm\sigma} = \Gamma_0(1 \pm P)$ for the parallel alignment of the magnetization on the two electrodes. Also two values of the intradot Coulomb correlation are used 0.05 eV and 0.2 eV in the absence of bias voltage ($eV_b = 0$) and with $J = 0$.

As we mentioned, our program calculate the values of the "molecular levels" self-consistently. Figsures 2 and 3 show the molecular levels, $+(-)$ performed the antibonding (bonding) states, keeping in mind that $E_1 = E_2$. The two parallel lines represent the spin-dependent chemical potential, which coincide in the case of magnetic parallel configuration. Fig. (2) shows the effective values of E_i for $P = 0.3$, that are lying in the energy window to be $-0.3 \leq E_i\ (\text{eV}) \leq -0.173$ and $0.124 \leq E_i\ (\text{eV}) \leq 0.247$ for $U_i = 0.05$ eV, while for $U_i = 0.2$ eV we have $-0.446 \leq E_i\ (\text{eV}) \leq -0.251$ and $0.05 \leq E_i\ (\text{eV}) \leq 0.246$. Table (1) introduces the active functional values of E_i (blue colored) and the corresponding range of the operative $E_{ij}^{\pm\sigma}$ values for the different values of U_i . Our calculations for $P = 0.7$ are presented in table (2).

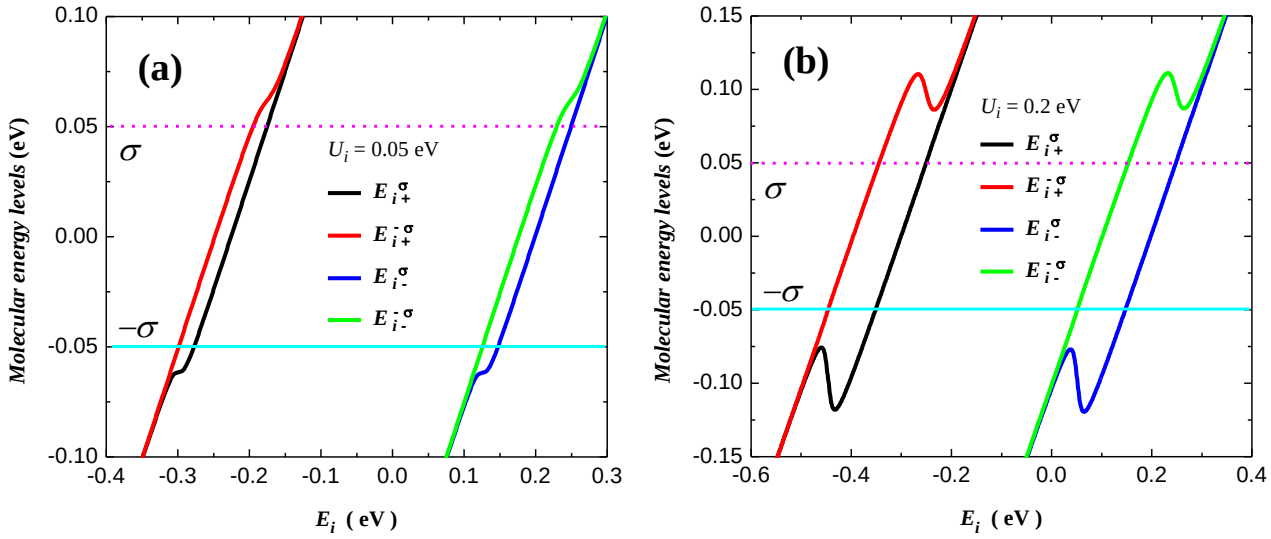

Figure 2: The molecular energy levels for ith QD as a function of E_i (eV) for different values of U_i (eV) with $P = 0.3$, $V_{12} = 0.2$ eV, $J = 0$, $T_L = T_R = 20$ K, $\Gamma_0 = 0.01$ eV, $\Gamma_{1L}^{\sigma} = \Gamma_{2R}^{\sigma} = 0.013$ eV, $\Gamma_{1L}^{-\sigma} = \Gamma_{2R}^{-\sigma} = 0.007$ eV.

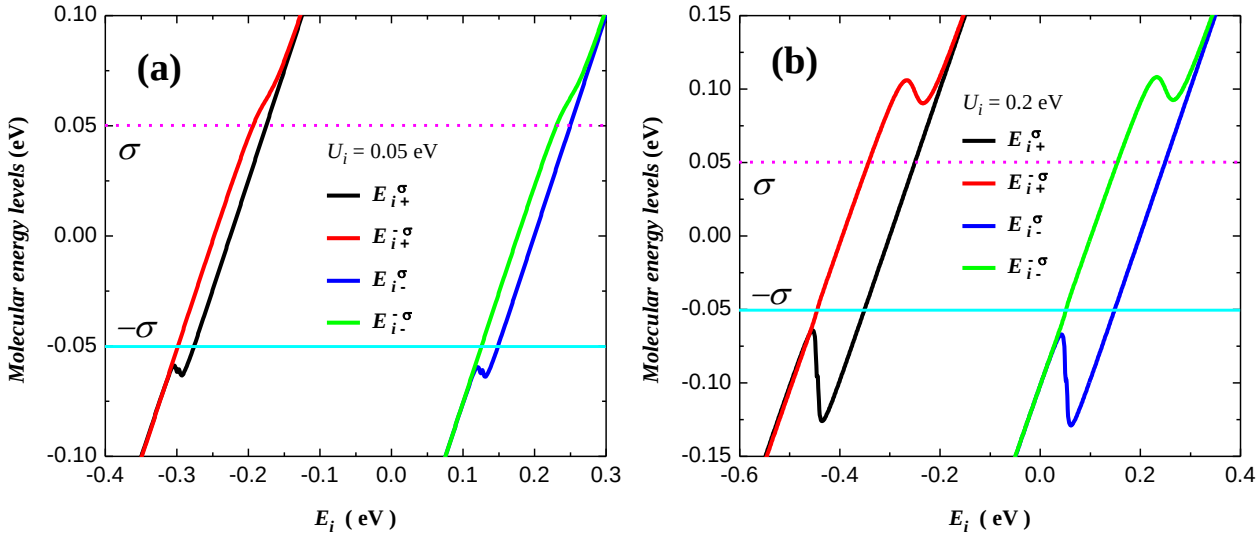

Figure 3: The molecular energy levels for ith QD as a function of E_i (eV) for different values of U_i (eV) with $P = 0.7$, $V_{12} = 0.2$ eV, $J = 0$, $T_L = T_R = 20$ K, $\Gamma_0 = 0.01$ eV, $\Gamma_{1L}^{\sigma} = \Gamma_{2R}^{\sigma} = 0.017$ eV, $\Gamma_{1L}^{-\sigma} = \Gamma_{2R}^{-\sigma} = 0.003$ eV.

Table 1: The active values of E_i and the corresponding operative values of $E_{ij}^{\pm\sigma}$ for $eV_b = 0$, $P = 0.3$, $J = 0$, $V_{12} = 0.2$ eV, $T_L = T_R = 20$ K, $\Gamma_0 = 0.01$ eV, $\Gamma_{1L}^{\sigma} = \Gamma_{2R}^{\sigma} = 0.013$ eV, $\Gamma_{1L}^{-\sigma} = \Gamma_{2R}^{-\sigma} = 0.007$ eV.

$U_i = 0.05$ eV				
E_i (eV)	E_{i+}^{σ} (eV)	$E_{i+}^{-\sigma}$ (eV)	E_{i-}^{σ} (eV)	$E_{i-}^{-\sigma}$ (eV)
-0.3	-0.0616	-0.05118	-0.4616	-0.45118
-0.173	0.05227	0.06289	-0.34773	-0.33711
0.124	0.33808	0.34839	-0.06192	-0.05161
0.248	0.44858	0.46153	0.04858	0.06153
$U_i = 0.2$ eV				
E_i (eV)	E_{i+}^{σ} (eV)	$E_{i+}^{-\sigma}$ (eV)	E_{i-}^{σ} (eV)	$E_{i-}^{-\sigma}$ (eV)
-0.446	-0.09762	-0.04974	-0.49762	-0.44973
-0.251	0.04951	0.09892	-0.35049	-0.30108
0.05	0.30562	0.34859	-0.09438	-0.05141
0.246	0.44778	0.50197	0.04778	0.10197

Table 2: The active values of E_i and the corresponding operative values of $E_{ij}^{\pm\sigma}$ for $eV_b = 0$, $P = 0.7$, $J = 0$, $V_{12} = 0.2$ eV, $T_L = T_R = 20$ K, $\Gamma_0 = 0.01$ eV, $\Gamma_{1L}^{\sigma} = \Gamma_{2R}^{\sigma} = 0.017$ eV, $\Gamma_{1L}^{-\sigma} = \Gamma_{2R}^{-\sigma} = 0.003$ eV.

$U_i = 0.05$ eV				
E_i (eV)	E_{i+}^{σ} (eV)	$E_{i+}^{-\sigma}$ (eV)	E_{i-}^{σ} (eV)	$E_{i-}^{-\sigma}$ (eV)
-0.3	-0.06159	-0.05153	-0.46159	-0.45153
-0.176	0.04911	0.0615	-0.35089	-0.3385
0.1239	0.33802	0.34821	-0.06198	-0.05179
0.248	0.44824	0.46157	0.04824	0.06157
$U_i = 0.2$ eV				
E_i (eV)	E_{i+}^{σ} (eV)	$E_{i+}^{-\sigma}$ (eV)	E_{i-}^{σ} (eV)	$E_{i-}^{-\sigma}$ (eV)
-0.447	-0.08847	-0.05213	-0.48847	-0.45213
-0.251	0.04921	0.09884	-0.35079	-0.30116
0.051	0.30122	0.34931	-0.09878	-0.05069
0.246	0.44675	0.50296	0.04675	0.10296

The blue colored values of $E_{i\pm}^{\pm\sigma}$ are the molecular levels that contribute in the quantum tunneling. As the quantum dots are symmetric, then $E_{1\pm}^{\pm\sigma} = E_{2\pm}^{\pm\sigma}$.

Figure 4a represents our calculations of the Seebeck coefficients (or thermopower) S^{σ} and $S^{-\sigma}$ as a function of the quantum dots effective energy levels (where $E_1 = E_2$). It is obvious that $S^{-\sigma} > S^{\sigma}$ for both values of U_i. This is consistent with the case $\Gamma_{i\alpha}^{\sigma} > \Gamma_{i\alpha}^{-\sigma}$. The values of E_i at which $S^{-\sigma}$ takes maximum values are -0.3 eV and 0.124 eV (-0.446 eV and 0.05 eV) for $U_i = 0.05$ eV ($U_i = 0.2$ eV). It is easy to notice that the energy spacing between the two Fano resonances when $U_i = 0.05$ eV is nearly equal to that when $U_i = 0.2$ eV. As U_i increases, the Fano resonances are shifted to the negative values of E_i. The serially coupled DQDs, which can be seen as a molecule with two energy states, bonding and antibonding states, causes the double Fano line shapes to appear. All the values of $S^{-\sigma}$ at Fano resonances are equal for both values of U_i. At the same mentioned values of E_i, one can notice the maximum values of charge Seebeck coefficient (see Fig. (4b)). At the same mentioned values of E_i (-0.446 eV, 0.05 eV when $U_i = 0.2$ eV and -0.3 eV, 0.124 eV, when $U_i = 0.05$ eV) one can notice the Fano antiresonances in Fig. 4c, where the spin Seebeck coefficient takes its maximum values in the vicinity of these antiresonances.

The dependence of the spin and charge Seebeck coefficients for thermospin conversion, on the QD energy level for $P = 0.7$ is plotted in Fig. 5, keeping in mind that $\Gamma_{i\alpha}^{\sigma}\ (P = 0.7) > \Gamma_{i\alpha}^{\sigma}\ (P = 0.3)$ and $\Gamma_{i\alpha}^{-\sigma}\ (P = 0.7) < \Gamma_{i\alpha}^{-\sigma}\ (P = 0.3)$. All values of S^{σ}, $S^{-\sigma}$, S_{ch} and S_{sp}, that are lying at the vicinity of Fano resonance and antiresonance respectively, are higher than that calculated for $P = 0.3$. It is obvious that S^{σ} and $S^{-\sigma}$ can be negative or positive value. When $E_i = 0$ and $P = 0.3$, it is confirmed that $S^{\sigma} < S^{-\sigma}$ which leads to the pure spin Seebeck effect without the charge Seebeck effect for $U_i = 0.05$ eV. According to the formula for the molecular levels, when $E_i = 0$, the spin-down and spin-up levels are asymmetric about the chemical potential $\mu = 0$, which leads to the pure spin Seebeck contribution. As a result, this system can generate spin-polarized current. The vanished values of S^{σ}, $S^{-\sigma}$, S_{ch} and S_{sp}, are referred to destructive quantum interference effect. The maximum values of S^{σ}, $S^{-\sigma}$, S_{ch} and S_{sp}, are lying in the vicinity of $E_i = -0.3$ eV for $U_i = 0.05$ eV and $E_i = 0.05$ eV for $U_i = 0.2$ eV. As a result, the spin and charge Seebeck effect can be enhanced by increasing U_i and P.

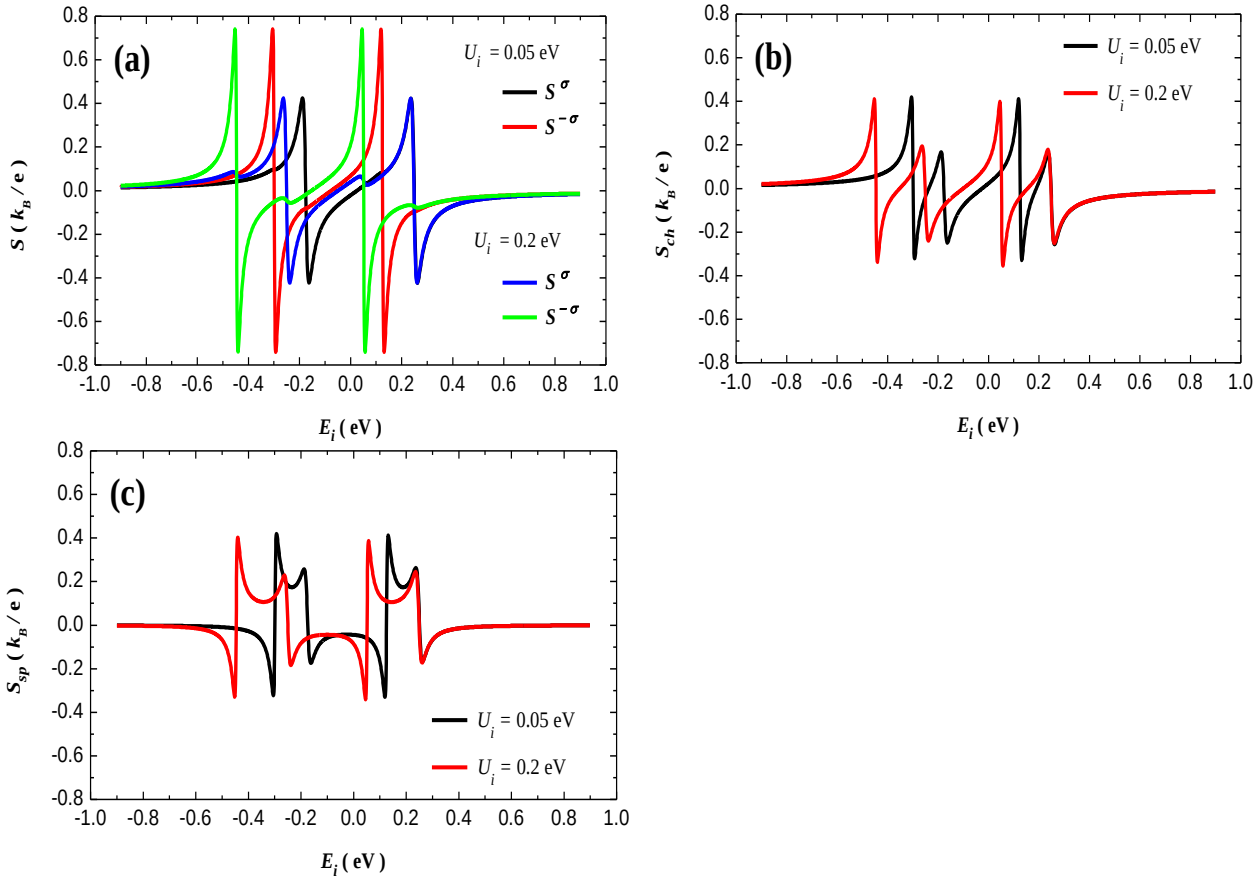

Figure 4: (a) The components of thermopower, (b) charge thermopower (c) spin thermopower as a function of E_i (eV) for different values of U_i (eV) with $P = 0.3$, $V_{12} = 0.2$ eV, $J = 0$, $T_L = T_R = 20$ K, $\Gamma_0 = 0.01$ eV, $\Gamma_{1L}^{\sigma} = \Gamma_{2R}^{\sigma} = 0.013$ eV, $\Gamma_{1L}^{-\sigma} = \Gamma_{2R}^{-\sigma} = 0.007$ eV.

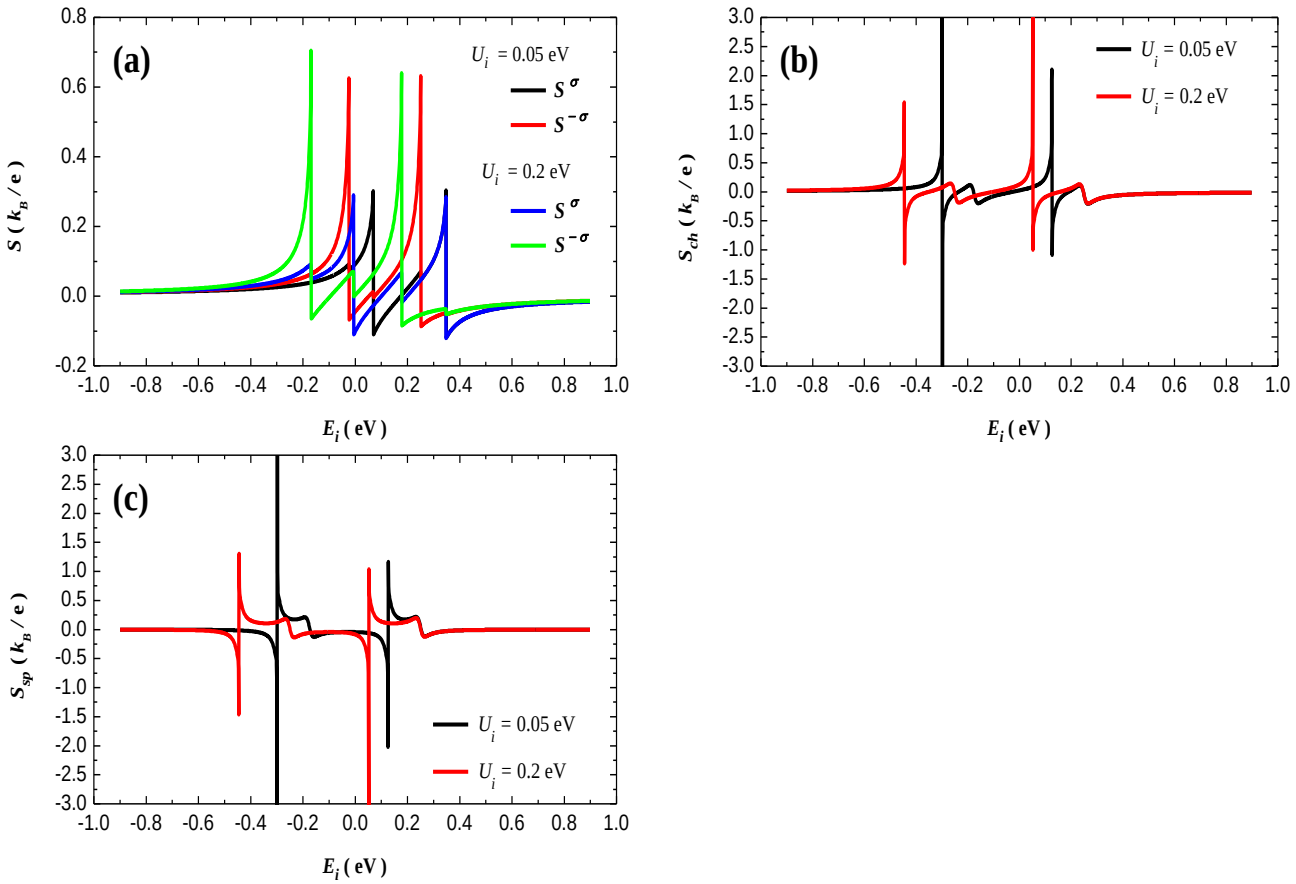

Figure 5: (a) The components of thermopower, (b) charge thermopower (c) spin thermopower as a function of E_i (eV) for different values of U_i (eV) with $P = 0.7$, $V_{12} = 0.2$ eV, $J = 0$, $T_L = T_R = 20$ K, $\Gamma_0 = 0.01$ eV, $\Gamma_{1L}^{\sigma} = \Gamma_{2R}^{\sigma} = 0.017$ eV, $\Gamma_{1L}^{-\sigma} = \Gamma_{2R}^{-\sigma} = 0.003$ eV.

The spin-dependent conductance G^{σ} and $G^{-\sigma}$ shows two peaks for each spin and intradot Coulomb correlation (see Fig. (6a)). These peaks are different in their height and width. The peaks of G^{σ} are greater (with wider width) than that of $G^{-\sigma}$. For each value of U_i, the charge conductance shows four peaks (see Fig. (6b)). In Fig. (6c), the spin conductance G_{sp} shows also four peaks for each U_i, this concides with the self-consistent solution of our model calculation. When U_i is increased, the molecular states of the spin-down and spin-up electrons are split, also the Fano resonance lines of G^{σ} and $G^{-\sigma}$ are split. For $P = 0.7$, $G^{-\sigma}$ for both values of U_i shows dips, while G^{σ} shows peaks (see Fig. (7)). This means that the quantum interference effect in channels σ and $-\sigma$ are different. The values of E_i that are corresponding to the dips are well illustrated in Fig. (7) b and c. It is found that the Fano dip of G^{σ} is in the closeness of the Fano peak of $G^{-\sigma}$ in Fig. (7a), leading to the generation of spin conductance G_{sp}. Correspondingly, the value of G_{ch} is reduced, as compared with the value of G_{sp}. It is concluded that the conductance

is not enhanced by the spin-polarization on the leads as well as by Coulomb correlation for both spin channels.The thermal conductance calculation is well presented in Figs. (8) and (9). These figures verify that the thermal conductance increases when the spin-polarization increases only when $E_i = -0.3$ eV with $U_i = 0.05$ eV as well as when $E_i = 0.05$ eV with $U_i = 0.2$ eV. Accordingly, at these values of E_i, the figure of merit will be decreases. These features are well explained in Figs. (10) and (11). Fig. (10) confirms that both the charge and spin figure of merit can be enhanced by lowering the Coulomb correlations with increasing the spin-polarization.

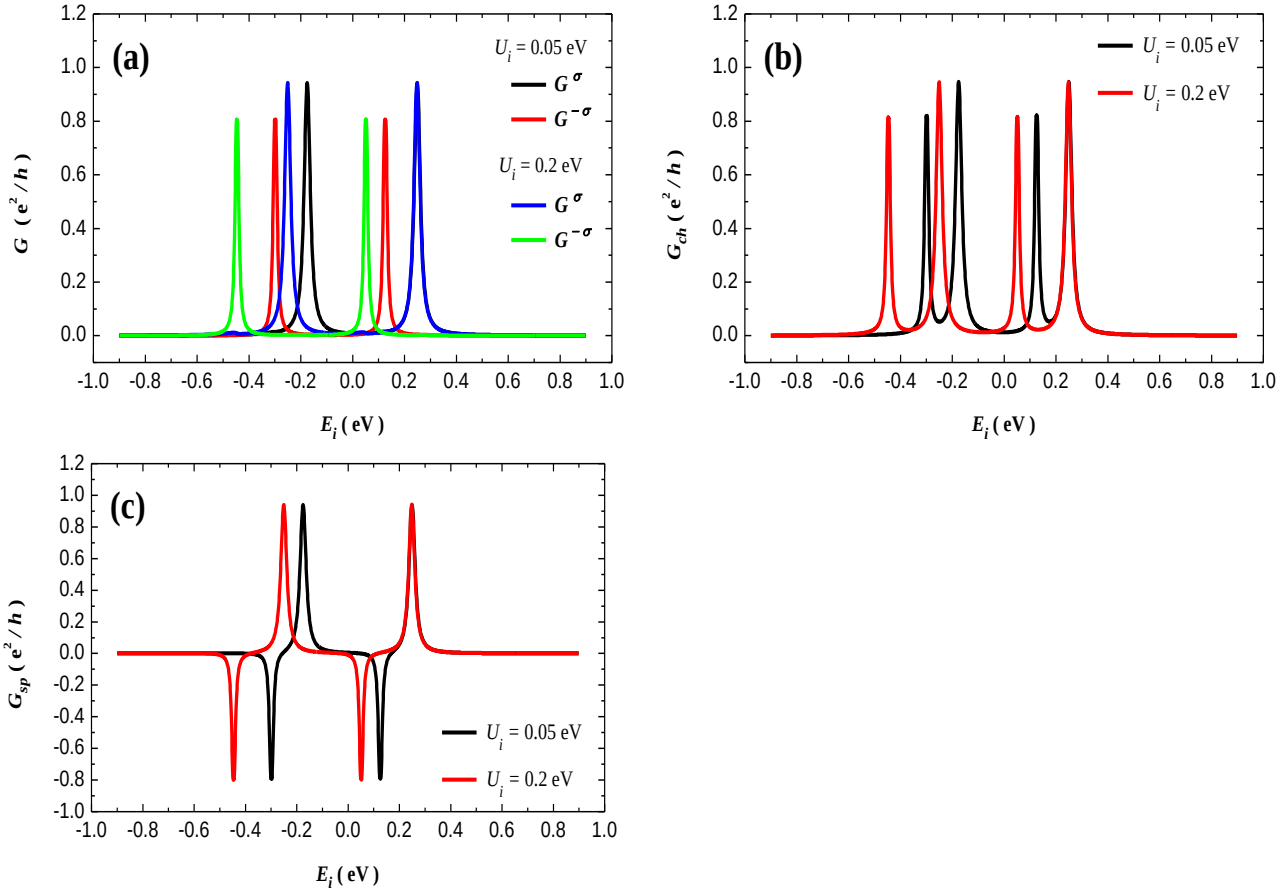

Figure 6: (a) The components of conductance, (b) charge conductance (c) spin conductance as a function of E_i (eV) for different values of U_i (eV) with $P = 0.3$, $V_{12} = 0.2$ eV, $J = 0$, $T_L = T_R = 20$ K, $\Gamma_0 = 0.01$ eV, $\Gamma_{1L}^{\sigma} = \Gamma_{2R}^{\sigma} = 0.013$ eV, $\Gamma_{1L}^{-\sigma} = \Gamma_{2R}^{-\sigma} = 0.007$ eV.

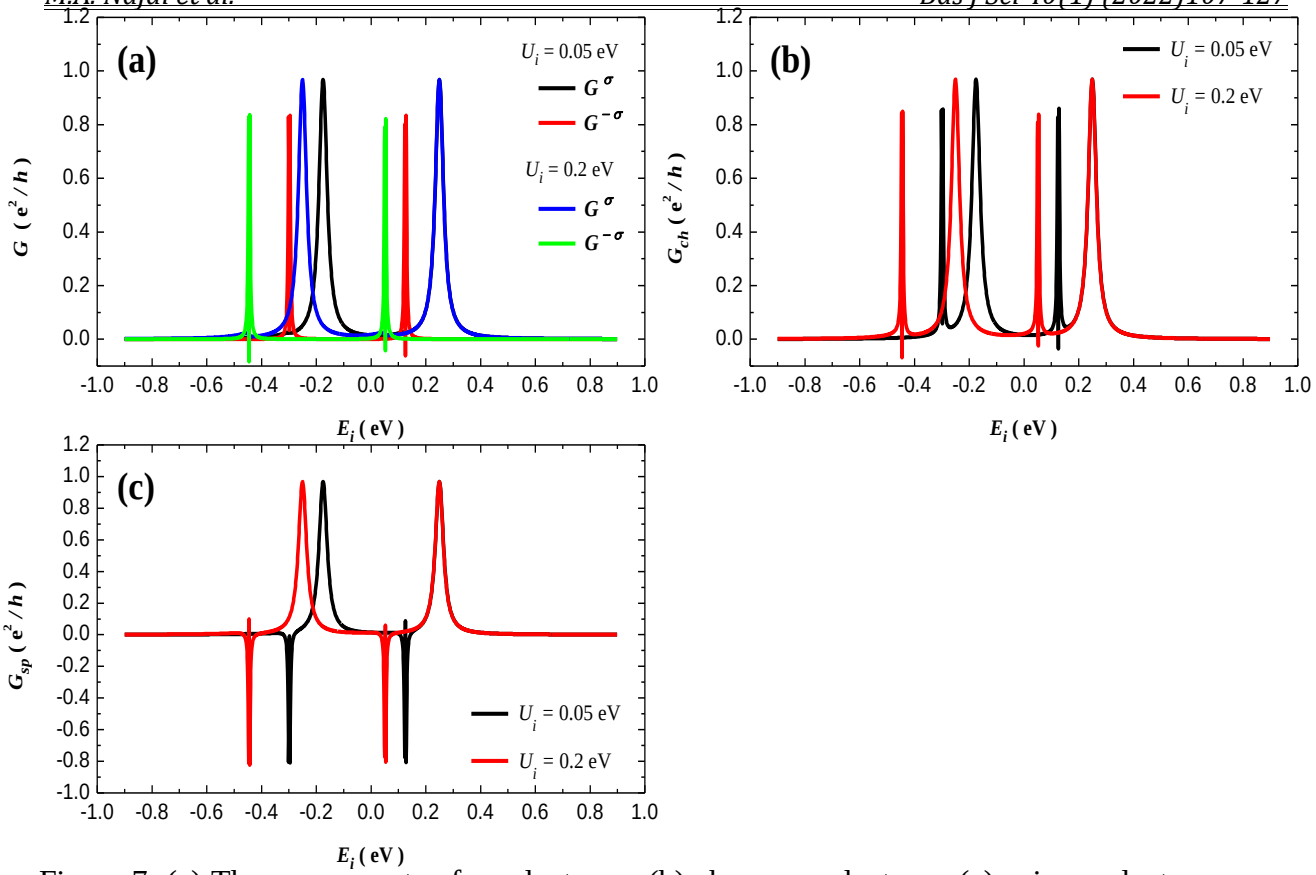

Figure 7: (a) The components of conductance, (b) charge conductance (c) spin conductance as a function of E_i (eV) for different values of U_i (eV) with $P = 0.7$, $V_{12} = 0.2$ eV, $J = 0$, $T_L = T_R = 20$ K, $\Gamma_0 = 0.01$ eV, $\Gamma_{1L}^{\sigma} = \Gamma_{2R}^{\sigma} = 0.017$ eV, $\Gamma_{1L}^{-\sigma} = \Gamma_{2R}^{-\sigma} = 0.003$ eV.

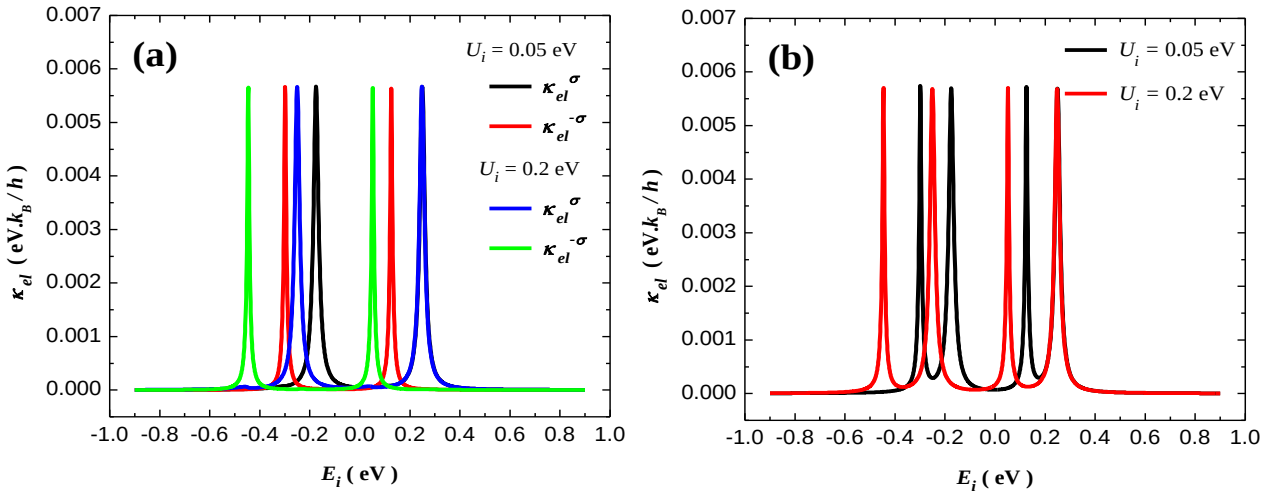

Figure 8: (a) The components of thermal conductance, (b) charge thermal conductance (c) spin thermal conductance as a function of E_i (eV) for different values of U_i (eV) with $P = 0.3$, $V_{12} = 0.2$ eV, $J = 0$, $T_L = T_R = 20$ K, $\Gamma_0 = 0.01$ eV, $\Gamma_{1L}^{\sigma} = \Gamma_{2R}^{\sigma} = 0.013$ eV, $\Gamma_{1L}^{-\sigma} = \Gamma_{2R}^{-\sigma} = 0.007$ eV.

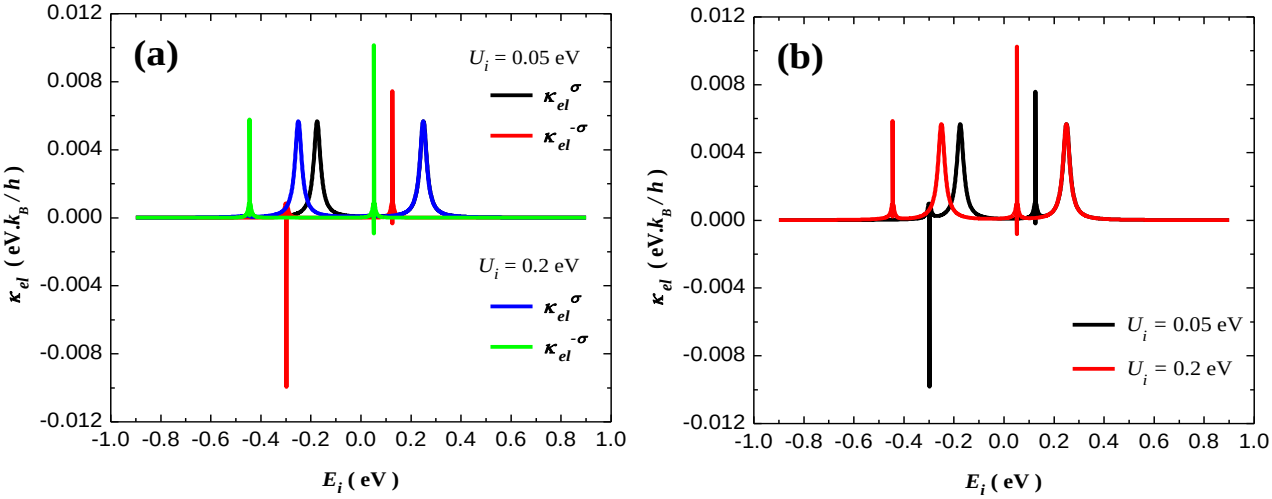

Figure 9: (a) The components of thermal conductance, (b) charge thermal conductance (c) spin thermal conductance as a function of E_i (eV) for different values of U_i (eV) with $P = 0.7$, $V_{12} = 0.2$ eV, $J = 0$, $T_L = T_R = 20$ K, $\Gamma_0 = 0.01$ eV, $\Gamma_{1L}^{\sigma} = \Gamma_{2R}^{\sigma} = 0.017$ eV, $\Gamma_{1L}^{-\sigma} = \Gamma_{2R}^{-\sigma} = 0.003$ eV.

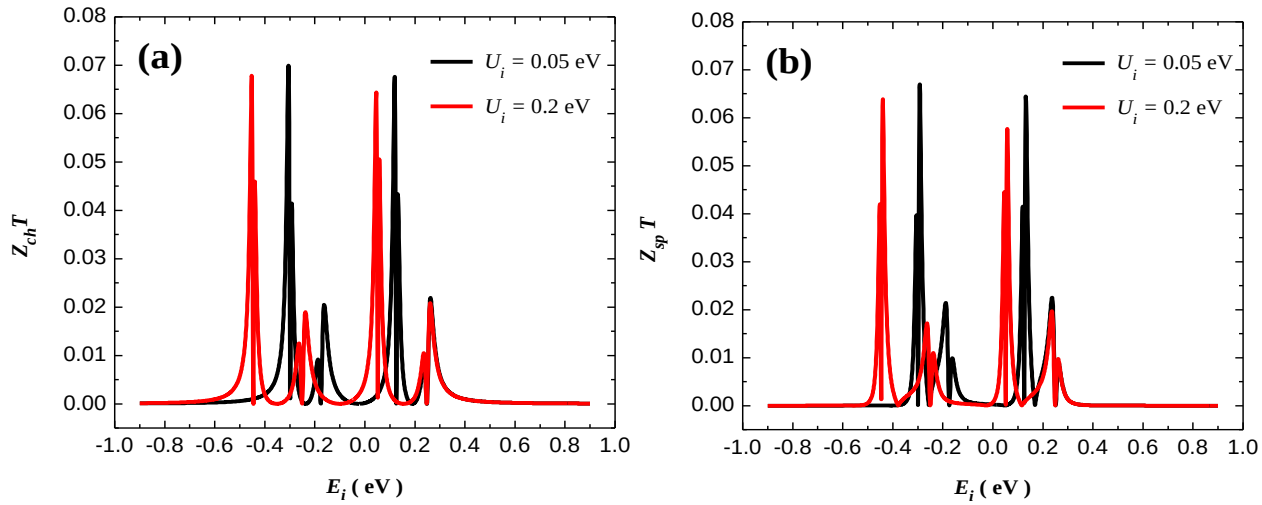

Figure 10: (a) Charge figure of merit (b) spin figure of merit as a function of E_i (eV) for different values of U_i (eV) with $P = 0.3$, $V_{12} = 0.2$ eV, $J = 0$, $T_L = T_R = 20$ K, $\Gamma_0 = 0.01$ eV, $\Gamma_{1L}^{\sigma} = \Gamma_{2R}^{\sigma} = 0.013$ eV, $\Gamma_{1L}^{-\sigma} = \Gamma_{2R}^{-\sigma} = 0.007$ eV.

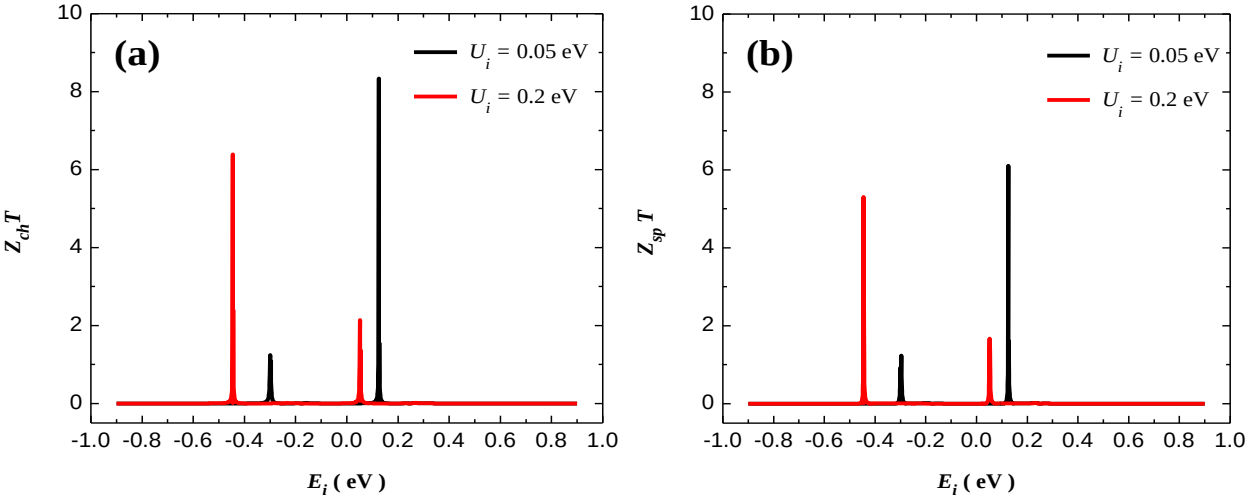

Figure 11: (a) Charge figure of merit (b) spin figure of merit as a function of E_i (eV) for different values of U_i (eV) with $P = 0.7$, $V_{12} = 0.2$ eV, $J = 0$, $T_L = T_R = 20$ K, $\Gamma_0 = 0.01$ eV, $\Gamma_{1L}^{\sigma} = \Gamma_{2R}^{\sigma} = 0.017$ eV, $\Gamma_{1L}^{-\sigma} = \Gamma_{2R}^{-\sigma} = 0.003$ eV.

4. Conclusions

In summary, we have studied the spin and charge thermoelectric properties across DQDs in the strong coupling regime (where $V_{12} > \Gamma_{i\alpha}^{\pm\sigma}$) in the case of parallel magnetic configuration. Using the nonequilibrium Green's function method and Sommerfeld expansion, the molecular levels are calculated self-consistently. We investigated how the intradot Coulomb correlation and spin-polarization influence the charge and spin thermoelectric properties through our system. In conclusion, when $E_i = 0$, the spin-down and spin-up levels are not symmetric about the chemical potential $\mu = 0$, which leads to the pure spin Seebeck contribution. As a result, this system can generate spin-polarized current when the spin-polarization on the lead is relatively high. Our calculations show that the value of the spin figure of merit is enhanced by increasing the spin-polarization and decreasing the correlation energy. These results can be utilize in spin and energy applications by using double quantum dots structure. It is profitable to submit an experimental scheme to test our results.

References

[1] A.A. Hashim, T.A. Selman, Tunneling Current calculation in double quantum dots, Basrah J. Sci. 36(2018)16-28, Iraqi Academic Scientific Journals - IASJ

[2] H. Jouhara, N. Khordehgah, S. Almahmoud, B. Delpech, A. Chauhan, S.A. Tassou, Waste heat recovery technologies and applications, Therm. Sci. Eng. Prog., 6(2018)268–289, https://doi.org/10.1016/j.tsep.2018.04.017

[3] H. Lu, Z. Huang, M.S. Martinez, J.C. Johnson, J.M. Luther, M.C. Beard, Transforming energy using quantum dots, Energy Environ. Sci., 13(2020)1347-1376, https://doi.org/10.1039/C9EE03930A

[4] I. Bashir, E. Blokhina, A. Esmailiyan, D. Leipold, M. Asker, E. Koskin, P. Giounanlis, H. Wang, D. Andrade-Miceli, A. Sokolov, A single-electron injection device for CMOS charge qubits implemented in 22-nm FD-SOI, IEEE Solid-State Circuits Lett., 3(2020)206-209. https://doi.org/10.1109/LSSC.2020.3010822

[5] D.M.T. Kuo, Y.-C. Chang, Effects of interdot hopping and Coulomb blockade on the thermoelectric properties of serially coupled quantum dots, Nanoscale Res. Lett., 7 (2012) 1-6. https://doi.org/10.1186/1556-276X-7-257

[6] S. Dong, Z.P. Niu, Thermospin effects in a quantum dot connected to normal leads, Phys. Lett. A, 379(2015)443-447, https://doi.org/10.1016/j.physleta.2014.11.048

[7] A. Svilans, M. Leijnse, H. Linke, Experiments on the thermoelectric properties of quantum dots, Comptes Rendus Phys., 17(2016)1096-1108, https://doi.org/10.1016/j.crhy.2016.08.002

[8] N.A. Zimbovskaya, Thermoelectric properties of a double-dot system in serial configuration within the Coulomb blockade regime, J. Chem. Phys., 153(2020)124712, https://doi.org/10.1063/5.0021260

[9] S. Dorsch, A. Svilans, M. Josefsson, B. Goldozian, M. Kumar, C. Thelander, A. Wacker, A. Burke, Heat driven transport in serial double quantum dot devices, Nano Lett., 21(2021)988-994, https://doi.org/10.1021/acs.nanolett.0c04017

[10] Y. Mazal, Y. Meir, Y. Dubi, Nonmonotonic thermoelectric currents and energy harvesting in interacting double quantum dots, Phys. Rev. B, 99(2019)75433, https://doi.org/10.1103/PhysRevB.99.075433

[11] F. Chi, Z.-G. Fu, L. Liu, P. Zhang, Enhanced spin-dependent thermopower in a double-quantum-dot sandwiched between two-dimensional electron gases, Chinese Phys. B, 28(2019)107305, http://dx.doi.org/10.1088/1674-1056/ab3f98

[12] A.A. Aligia, D.P. Daroca, L. Arrachea, P. Roura-Bas, Heat current across a capacitively coupled double quantum dot, Phys. Rev. B, 101(2020)75417, https://doi.org/10.1103/PhysRevB.101.075417

[13] Z. Li, Y. Cheng, J. Wei, X. Zheng, Y. Yan, Kondo-peak splitting and resonance

enhancement caused by interdot tunneling in coupled double quantum dots, Phys. Rev. B, 98(2018)115133, https://doi.org/10.1103/PhysRevB.98.115133

[14] M.A. Sierra, R. López, J.S. Lim, Thermally Driven Out-of-Equilibrium Two-Impurity Kondo System, Phys. Rev. Lett., 121(2018)96801, https://doi.org/10.1103/PhysRevLett.121.096801

[15] H.K. Yadalam, U. Harbola, Statistics of heat transport across a capacitively coupled double quantum dot circuit, Phys. Rev. B, 99(2019)195449 https://doi.org/10.1103/PhysRevB.99.195449

[16] G.E.W. Bauer, E. Saitoh, B.J. Van Wees, Spin caloritronics, Nat. Mater., 11(2012)391-399, https://doi.org/10.1038/NMAT3301

[17] X.-Q. Yu, Z.-G. Zhu, G. Su, A.-P. Jauho, Spin-caloritronic batteries, Phys. Rev. Appl., 8(2017)54038, https://doi.org/10.1103/PhysRevApplied.8.054038

[18] L.-L. Nian, W. Liu, L. Bai, X.-F. Wang, Spin caloritronics in a chiral double-strand-DNA-based hybrid junction, Phys. Rev. B, 99(2019)195430 https://doi.org/10.1103/PhysRevB.99.195430

[19] N. Marchal, T. da C.S.C. Gomes, F.A. Araujo, L. Piraux, Large spin-dependent thermoelectric effects in NiFe-based interconnected nanowire networks, Nanoscale Res. Lett., 15(2020)1-8, https://doi.org/10.1186/s11671-020-03343-8

[20] Z. Gholami, F. Khoeini, Vacancy tuned thermoelectric properties and high spin filtering performance in graphene/silicene heterostructures, Sci. Rep., 11(2021)1-14, https://doi.org/10.1038/s41598-021-94842-w

[21] J.-S. Wang, B.K. Agarwalla, H. Li, J. Thingna, Nonequilibrium Green's function method for quantum thermal transport, Front. Phys., 9(2014)673-697, https://doi.org/10.1007/s11467-013-0340-x

[22] D.M.-T. Kuo, S.-Y. Shiau, Y. Chang, Theory of spin blockade, charge ratchet effect, and thermoelectrical behavior in serially coupled quantum dot system, Phys. Rev. B, 84(2011) 245303, https://doi.org/10.1103/PhysRevB.84.245303

[23] J.W. Gadzuk, J.K. Hartman, T.N. Rhodin, Approach to alkali-metal chemisorption within the Anderson model, Phys. Rev. B, 4(1971)241, https://doi.org/10.1103/PhysRevB.4.241

[24] M.K. Shamer, Heat current rectification in a single quantum dot system with the presence and absence of the magnetic field, Indian J. Phys.,(2021)1-6, https://doi.org/10.1007/s12648-021-02161-7

[25] M.A. Najdi, H.A. Jassem, J.M. AL-Mukh, Electron tunneling through serially coupled double quantum dots: The Coulomb blockade, IOP Conf. Ser. Mater. Sci. Eng., 454(2018) 012043, https://doi.org/10.1088/1757-899X/454/1/012043

[26] T. Fukadai, T. Sasamoto, Transient dynamics of double quantum dots coupled to two reservoirs, J. Phys. Soc. Japan., 872018)54006, https://doi.org/10.7566/JPSJ.87.054006

[27] Y.S. Liu, X.F. Yang, X.K. Hong, M.S. Si, F. Chi, Y. Guo, A high-efficiency double

quantum dot heat engine, Appl. Phys. Lett., 103(2013)93901, https://doi.org/10.1063/1.4819852

[28] X. Zhou, F. Qi, G. Jin, Enhanced spin figure of merit in an Aharonov-Bohm ring with a double quantum dot, J. Appl. Phys., 115(2014)153706. https://doi.org/10.1063/1.4871542

[29] M.A. Najdi, J.M. Al-Mukh, H.A. Jassem, Model Parameterization for Coherent Manipulation in Spin Current through FM-QD1-QD2-FM, J. Phys. Conf. Ser., 1818(2021) 012102, https://doi.org/10.1088/1742-6596/1818/1/012102

[30] M.A. Najdi, J.M. Al-Mukh, H.A. Jassem, Theoretical Investigation in Coherent Manipulation throughout the Calculation of the Local Density of States in FM-DQD-FM Device, Mater. Sci. Forum, Trans Tech Publ., 1039(2021)451-469, https://doi.org/10.4028/www.scientific.net/MSF.1039.451

[31] Y. Dai, X.-F. Wang, P. Vasilopoulos, Y.-S. Liu, Tunable spin-polarized transport through a side-gated double quantum dot molecular junction in the Coulomb blockade regime, Appl. Nanosci., 9(2019)1685-1693, https://doi.org/10.1007/s13204-019-00981-y

[32] S.-C. Yu, F. Chi, L.-M. Liu, H. Chen, Enhanced Spin Seebeck Efficiency in Closed Triple Quantum Dots Ring with Spin-Dependent Interdot Couplings, Int. J. Theor. Phys., 58(2019)2757-2769, https://doi.org/10.1007/S10773-019-04106-7

[33] Y. Kleeorin, Y. Meir, Quantum phase transition in a realistic double-quantum-dot system, Sci. Rep., 8(2018)1-7, https://doi.org/10.1038/s41598-018-28822-y

[34] T.A. Costi, V. Zlatić, Thermoelectric transport through strongly correlated quantum dots, Phys. Rev. B, 81(2010)235127, https://doi.org/10.1103/PhysRevB.81.235127

[35] W. Qiang, X. Hai-Qing, J. Hu-Jun, L. Zhi-Jian, N. Yi-Hang, Spin-dependent thermoelectric transport through double quantum dots, Chinese Phys. B, 21(2012)117310, https://doi.org/10.1088/1674-1056/21/11/117310

[36] S. Donsa, S. Andergassen, K. Held, Double quantum dot as a minimal thermoelectric generator, Phys. Rev. B, 89 (2014)125103, https://doi.org/10.1103/PhysRevB.89.125103

[37] Ł. Karwacki, Spin Thermoelectric Effects in a Strongly Correlated Double Quantum Dot System., Acta Phys. Pol. A127(2015)1-13, https://doi.org/10.1103/PhysRevB.94.085418

[38] L.S. Ricco, F.A. Dessotti, I.A. Shelykh, M.S. Figueira, A.C. Seridonio, Tuning of heat and charge transport by Majorana fermions, Sci. Rep., 8(2018)1–8, https://doi.org/10.1038/s41598-018-21180-9

الخصائص الكهروحرارية للشحنة والبرم عبر نقطتين كميتين مقترنة تسلسلياً مع أقطاب فيرومغناطيسية: حالة التوزيع المغناطيسي المتوازي

محمد عبدالزهره نجدي[1] جنان مجيد المخ[2] هيفاء عبد النبي جاسم[1]

[1] قسم الفيزياء / كلية العلوم / جامعة البصرة / البصرة / العراق
[2] قسم الفيزياء / كلية التربية للعلوم الصرفة / جامعة البصرة / البصرة / العراق

المستخلص

في هذه المقالة ، تم دراسة الخواص الكهروحرارية للشحنة والبرم لنظام النقطتين الكميتين المتصلة بأقطاب فيرومغناطيسية مع توزيع مغناطيسي متوازي في نهج الاستجابة الخطية . تم حساب نتائجنا في نهج الاقتران القوي من خلال مراعاة جميع المعاملات التي تؤثر على النظام مثل الاقتران بين النقطتين الكميتين وكذلك مع الأقطاب ، طاقة تفاعل كولوم على النقاط الكمية واستقطاب البرم على الأقطاب . لقد وجد أنه في التوزيع المغناطيسي المتوازي ، يمكن أن تصل الكفاءة الكهروحرارية إلى قيمة كبيرة حول مستويات الرنين للبرم-اسفل عندما يكون اقتران النفق بين النقاط الكمية والأقطاب للإلكترونات ذات البرم-اسفل صغيرًا ، مما يؤدي إلى مساهمة سيبك البرمية النقية . نتيجة لذلك ، يمكن لهذا النظام أن يولد تيار برم مستقطب . يتم تعزيز قيمة شكل الكفاءة البرمية عن طريق زيادة استقطاب البرم وتقليل طاقة التفاعل.